



**AMS**  
American Meteorological Society

## Supplemental Material

© Copyright 2021 [American Meteorological Society](https://www.ametsoc.org) (AMS)

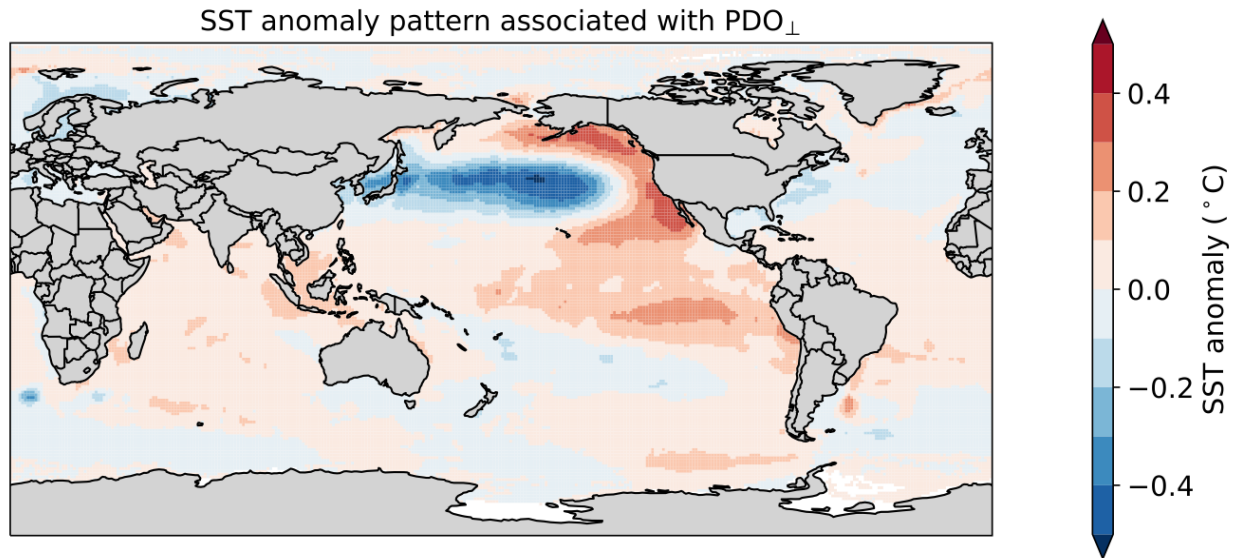
For permission to reuse any portion of this work, please contact [permissions@ametsoc.org](mailto:permissions@ametsoc.org). Any use of material in this work that is determined to be “fair use” under Section 107 of the U.S. Copyright Act (17 USC §107) or that satisfies the conditions specified in Section 108 of the U.S. Copyright Act (17 USC §108) does not require AMS’s permission. Republication, systematic reproduction, posting in electronic form, such as on a website or in a searchable database, or other uses of this material, except as exempted by the above statement, requires written permission or a license from AMS. All AMS journals and monograph publications are registered with the Copyright Clearance Center (<https://www.copyright.com>). Additional details are provided in the AMS Copyright Policy statement, available on the AMS website (<https://www.ametsoc.org/PUBSCopyrightPolicy>).

1 **Supplementary Figures for The inherent uncertainty of**  
2 **precipitation variability, trends, and extremes due to**  
3 **internal variability, with implications for Western US**  
4 **water resources**

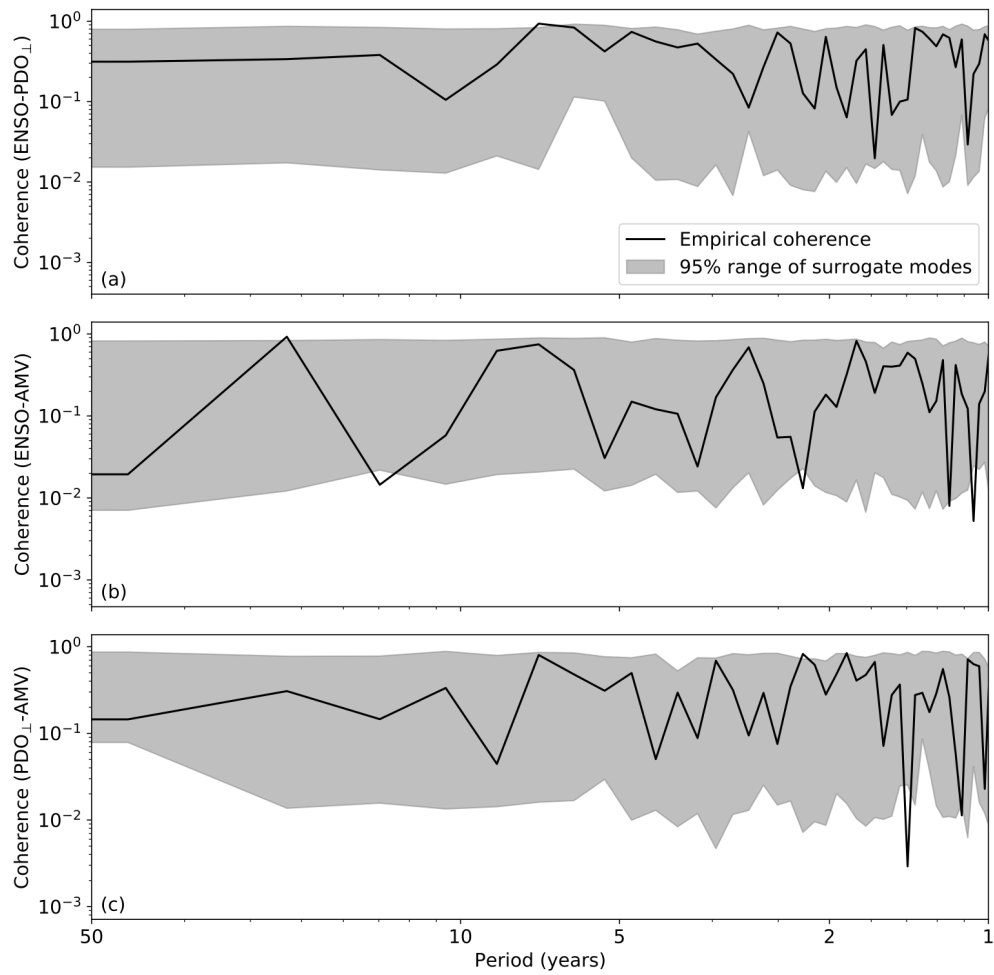
5 Karen A. McKinnon<sup>1\*</sup> and Clara Deser<sup>2</sup>

6 <sup>1</sup>Department of Statistics and Institute of the Environment and Sustainability; University  
7 of California, Los Angeles; Los Angeles, CA 90095; kmckinnon@ucla.edu

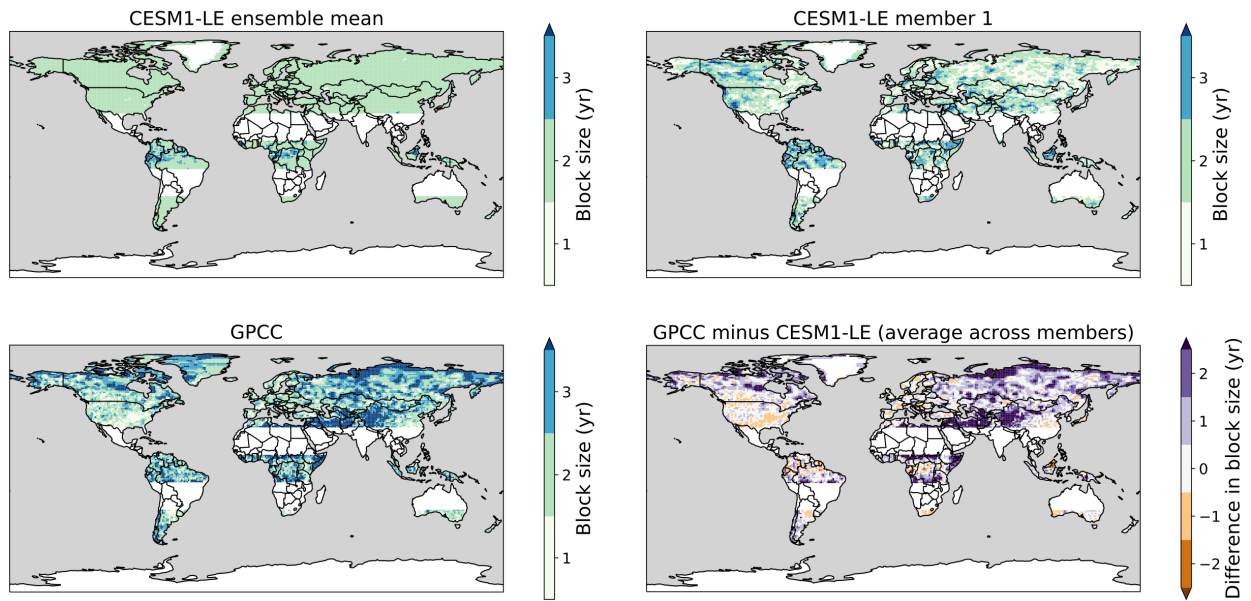
8 <sup>2</sup>National Center for Atmospheric Research; Boulder, CO 80305



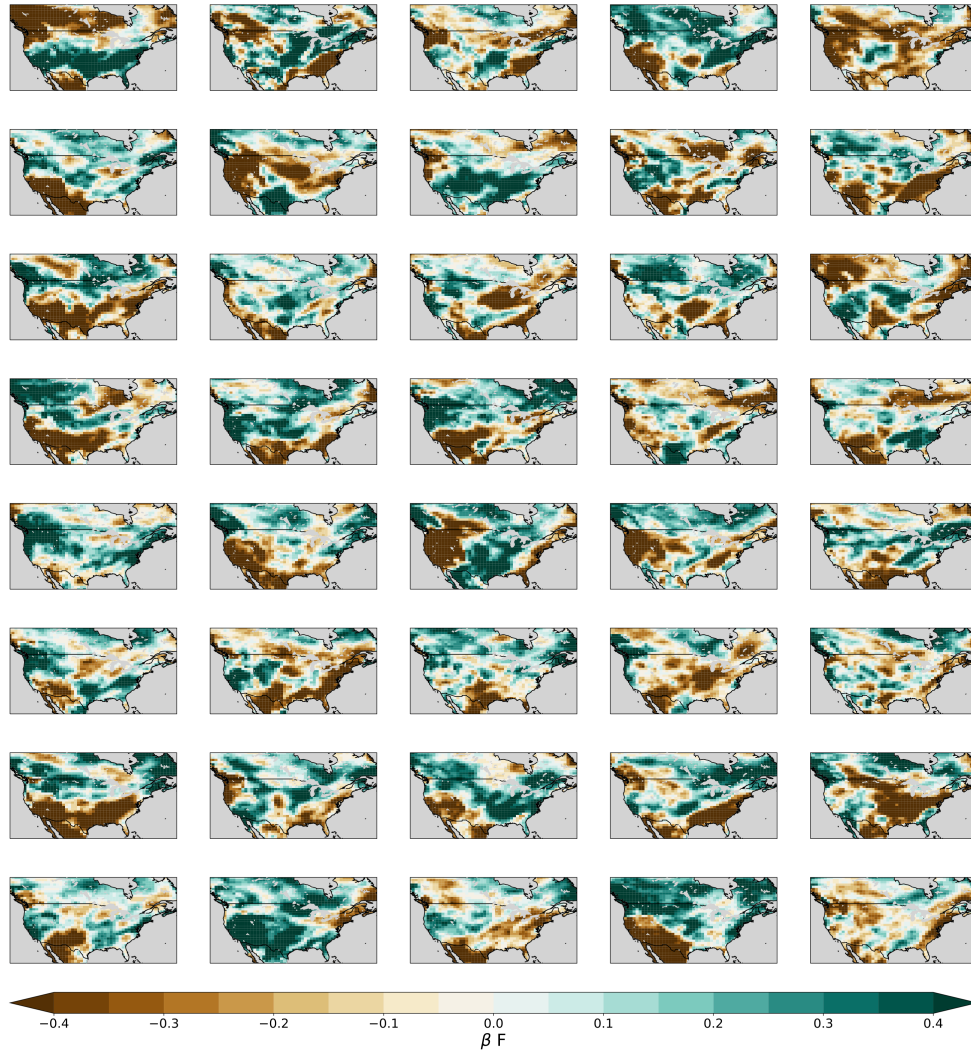
Supplementary Figure 1: The sea surface temperature (SST) anomaly pattern associated with  $\text{PDO}_{\perp}^t$ , the component of the traditional Pacific Decadal Oscillation time series that is orthogonal to the El Niño-Southern Oscillation time series. The SST anomaly pattern is calculated by regressing the annual mean  $\text{PDO}_{\perp}^t$  time series onto the annual mean, linearly detrended SST anomalies from HadISST.



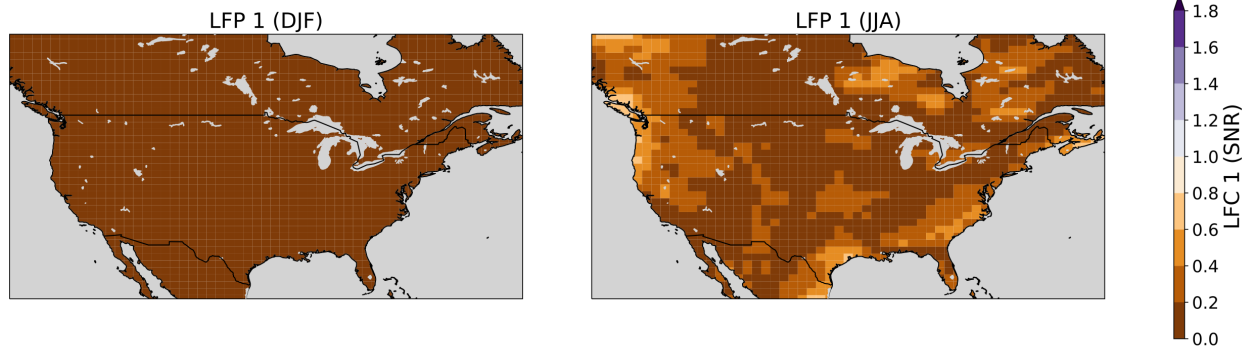
Supplementary Figure 2: The empirical coherence (black line) and 95% range of coherence values from the synthetic mode times series between (a) ENSO and PDO $_{\perp}$ , (b) ENSO and AMV, and (c) PDO $_{\perp}$  and AMV.



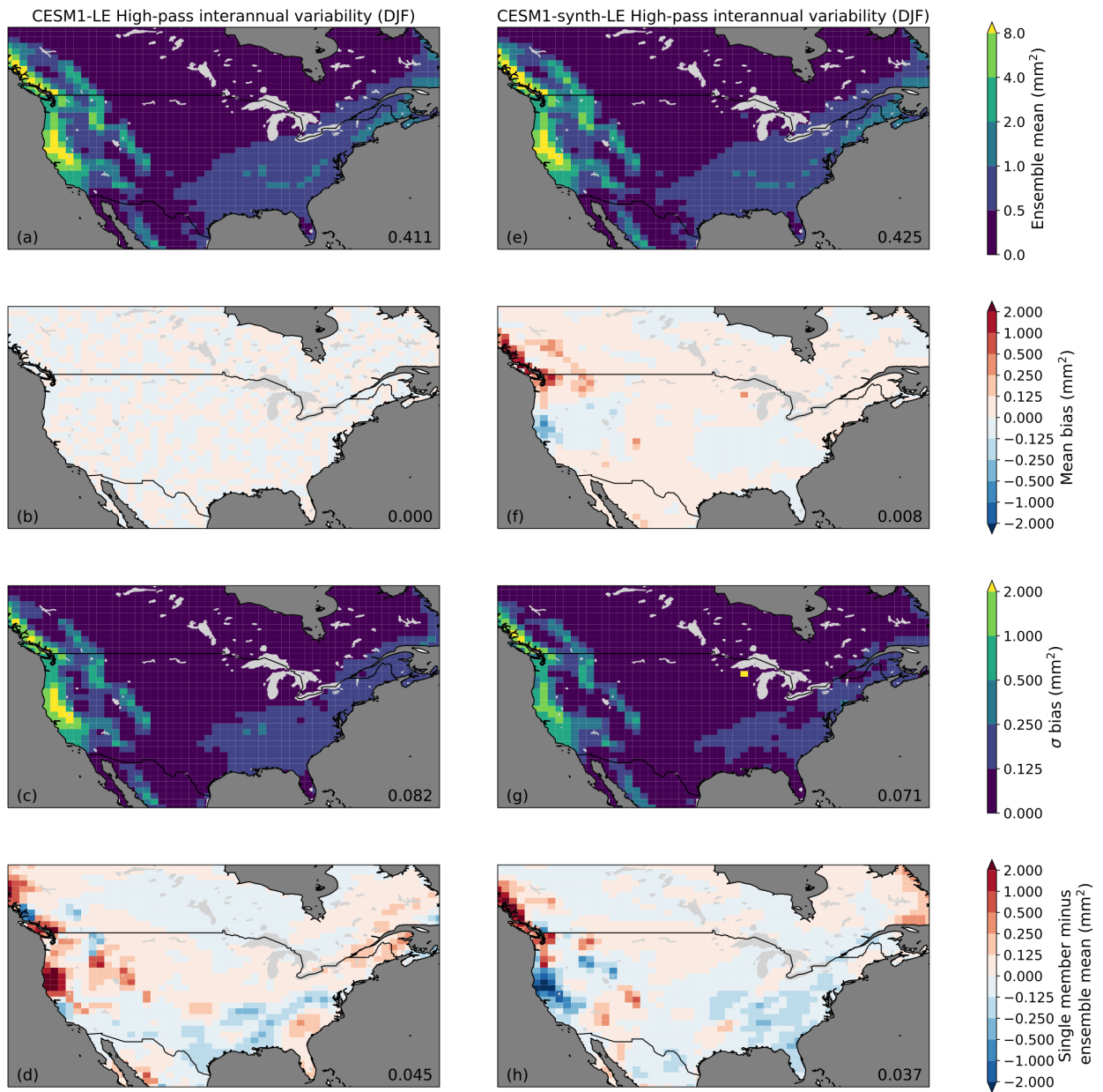
Supplementary Figure 3: The selected block size at each gridbox for CESM1-LE and the GPCCC observations. Block size is chosen for each gridbox and month using the methods of *Wilks* (1997); the maps show the maximum value across months. The CESM1-LE ensemble mean shows the average selected block size across members. Member 1 is shown as an example of the block size given a single record, which is more readily compared to the GPCCC-based observational estimate. The average across ensemble members of the difference between the GPCCC- and CESM1-based block sizes shows that, in most regions of the world outside of North America and Europe, the GPCCC dataset suggests a larger block size. The dry subtropics are excluded since some months climatologically have no rain.



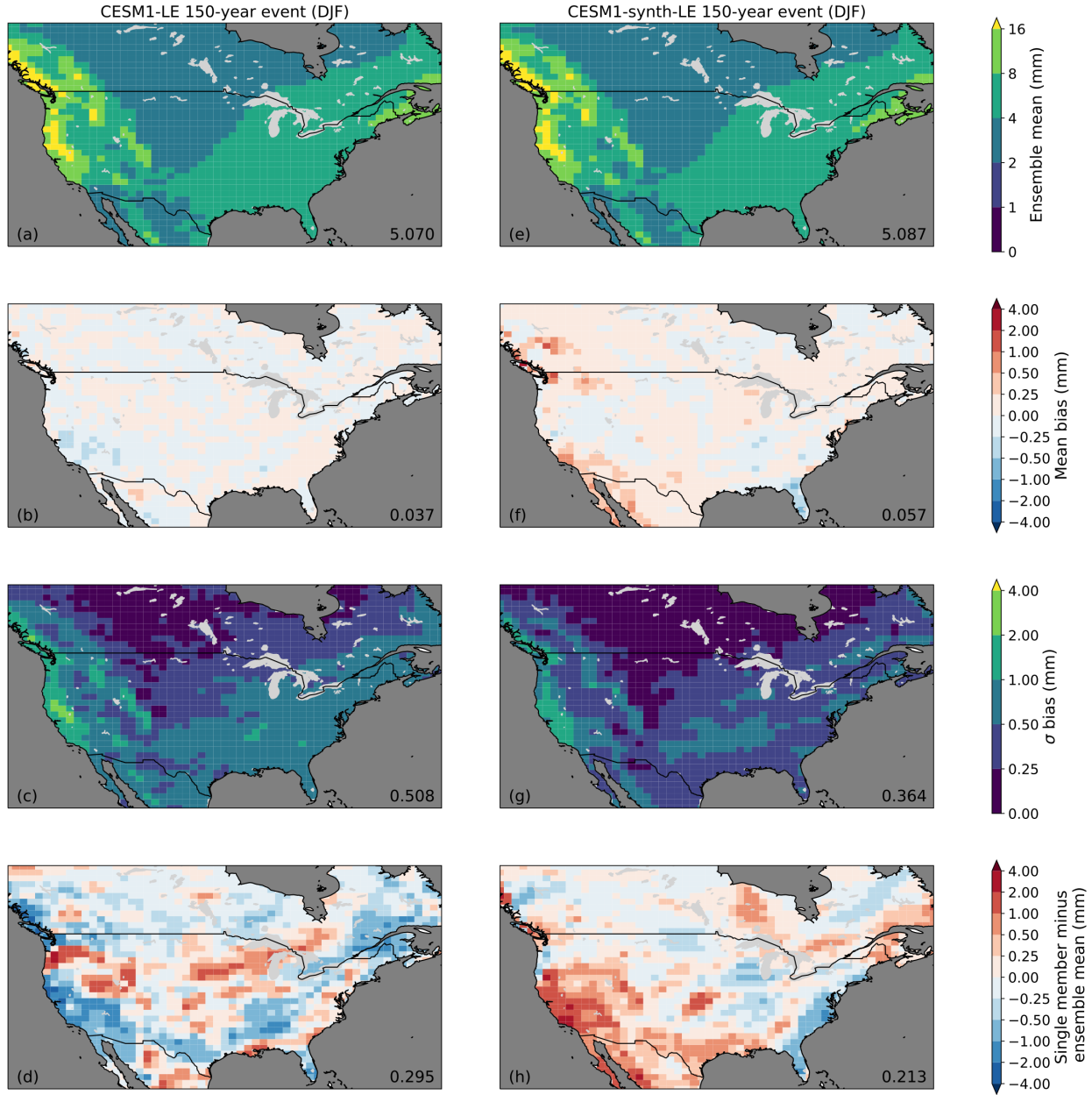
Supplementary Figure 4: The DJF-average value of  $\beta_F$  estimated in each member of the CESM1-LE independently. The large differences across maps indicates that the estimated forced component is being dominated by sampling of internal variability.



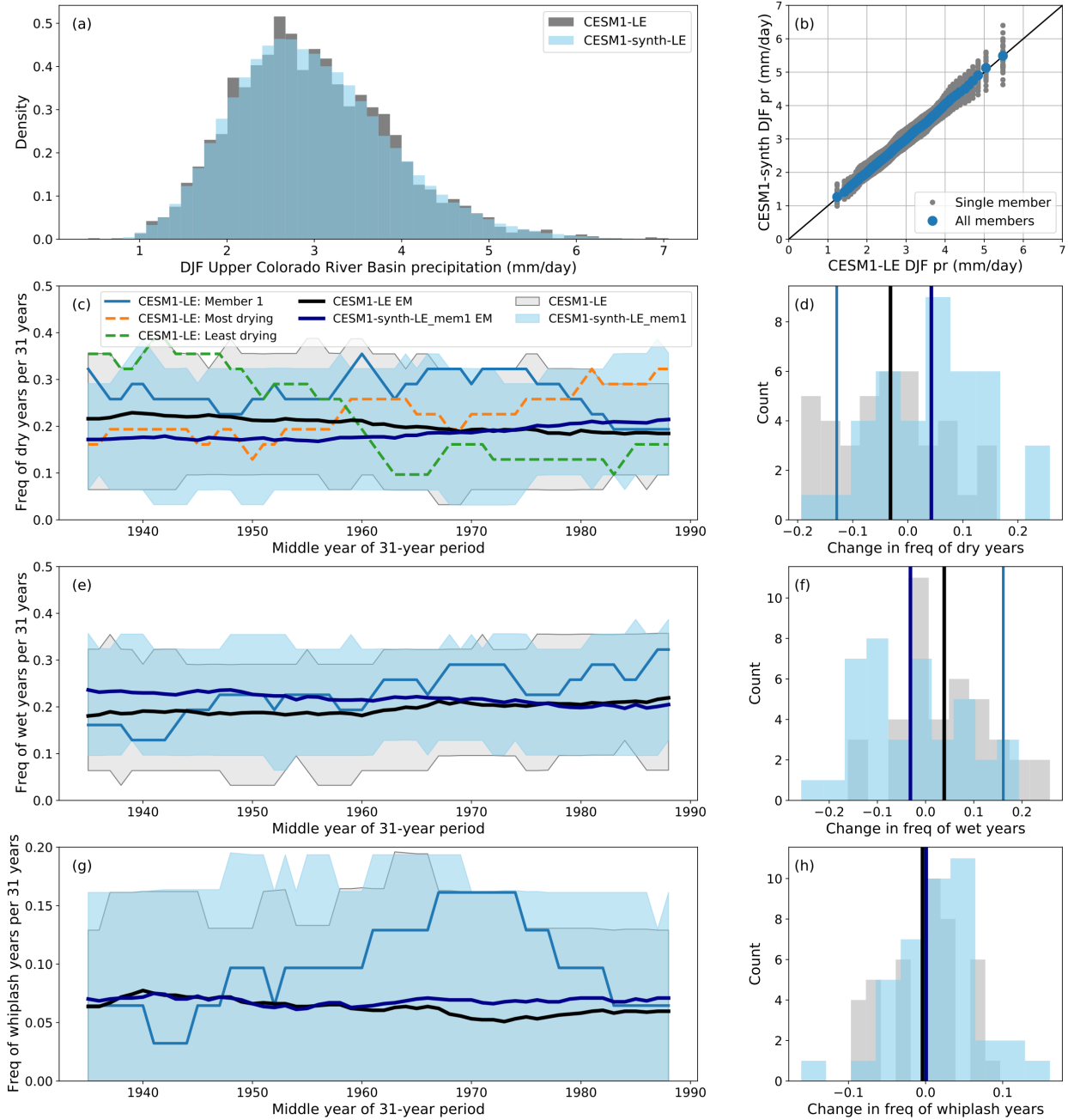
Supplementary Figure 5: The signal to noise ratio for the forced component for winter (left) and summer (right) estimated using low frequency component analysis (*Wills et al.* 2018). The forced component is assumed to be contained in the first low frequency pattern (LFP). The LFPs are estimated in each member of CESM1-LE as a linear combination of the first 30 EOFs for monthly precipitation. The signal is defined as the mean of the first LFP across the ensemble, and the noise is the standard deviation across the ensemble.



Supplementary Figure 6: As in Figure 6, but for high-frequency variability (frequency  $> 1/10\text{y}$ ).



Supplementary Figure 7: As in Figure 6, but for the magnitude of the 150-year event. Return periods are estimated empirically in each 85-year member of either the CSM1-LE or the CSM1-synth-LE as  $\frac{n+0.12}{m-0.44}$  (Gringorten, 1963), where  $n$  is the number of years in the record, and  $m$  is the rank of each event. While more sophisticated estimates of the probability of extremes are possible, such as by using extreme value theory, the simpler empirical approach is sufficient for our purposes of intercomparison between ensembles. When using the full CSM1-LE, which contains 3400 member-years, the choice of weighting scheme becomes irrelevant, and the 150-year event can be estimated as the 23rd most extreme value across the member-years. Comparing this estimate to the use of the Gringorten formula for each member individually shows that the Gringorten approximation for the 85-year records is largely unbiased (Panel b).



Supplementary Figure 8: Validation of the synthetic ensemble methodology for water resource metrics in the Upper Colorado River Basin (see outline in Figure 10). (a, b) The distribution of DJF Upper Colorado River Basin precipitation across the full CESM1-LE and CESM1-synth-LE. (c) The time series of the frequency of dry years in overlapping 31-year periods across the full CESM1-LE (black), the first member of the CESM1-LE (light blue), and the CESM1-synth-LE\_mem1, which is based on the first member of the CESM1-LE alone (dark blue). The 5%-95% range across the two ensembles is shown in gray for the CESM1-LE and light blue for the CESM1-synth-LE\_mem1. (d) The change in the frequency of dry years from the first (1921-1951) to the last (1985-2005) 31-year period. All colors are the same as in (c). (e, f) As in (c, d) but for wet years. (g, h) As in (c, d) but for whiplash years.

## 9 References

- 10 Gringorten, I. I. (1963), A plotting rule for extreme probability paper, *Journal of Geophysical*  
11 *Research*, 68(3), 813–814.